Molecular Dynamics Simulations of Dodecylphosphocholine Micelles at Three Different Aggregate Sizes: Micellar Structure and Chain Relaxation

D. P. Tieleman,*,† D. van der Spoel,‡ and H. J. C. Berendsen†

Department of Biophysical Chemistry, University of Groningen, Nijenborgh 4, 9747 AG Groningen, The Netherlands, and Department of Biochemistry, Biomedical Center, Husargaten 3, Box 576, 75123 Uppsala, Sweden

Received: April 3, 2000

We simulated micelles of 40 (M40), 54 (M54), and 65 (M65) dodecylphosphocholine (DPC) lipids in water for up to 15 ns and analyzed the system energetics, structure of the water/lipid interface, structure and dynamics of the lipid tails, and overall size and shape of the micelles. M54 and M65 are similar, being mostly spherical in shape with comparable tail order parameters, atom distributions, and solvent accessible areas, whereas M40 assumes a prolate ellipsoid shape with a larger hydrophobic solvent accessible area per lipid and more restricted lipid packing. A comparison of the lipid chain structure and dynamics with those of decane and dipalmitoylphosphatidylcholine (DPPC) shows that the trans dihedral fractions are comparable, but that the dihedral transition rate is considerably slower in the micelles than in decane or DPPC, in agreement with a previous simulation of the sodium dodecyl sulfate micelle but in contrast with a recent simulation of DPC. The relaxation behavior of the CH_2 segments in the lipid chains is complex, and the overall and internal motions of the lipids cannot be separated. The full orientational autocorrelation function of the CH vectors is calculated and found to decay to zero within a few nanoseconds, which is fast compared to overall micellar rotation. From a direct calculation of the spectral densities, ^{13}C T_1 and T_2 relaxation times of the tail carbons are calculated and found to agree well with experimental measurements for the lipid chain carbons, but less well for the headgroup.

1. Introduction

Micelles play an important role in biochemical techniques, such as solubilization and crystallization of membrane proteins,[1,2] and as models for a membrane environment of lipid-bound peptides using NMR measurements.[3,4] Dodecylphosphocholine (DPC) is a popular lipid used for these purposes because it resembles common phosphatidylcholine lipids.[5,6] It has been used in studies of peptides such as melittin,[5] cardiotoxin γ,[7] β-amyloid fragment,[8] and nisin.[9]

Micelles have been studied by a variety of methods. NMR relaxation measurements give effective relaxation times and order parameters for the carbon tails.[10−12] Neutron diffraction[13] and infrared spectroscopy[14] experiments provide low-resolution structural information on micelles. In addition, physicochemical techniques give average values for diffusion coefficients and aggregate sizes.[5,15] In recent years, several molecular dynamics studies of realistic micelles have provided a detailed picture of micelle dynamics for anionic (sodium dodecyl sulfate,[16] and octanoate[17,18]), cationic (*n*-decyltrimethylammonium chloride[19]), and reversed-anionic (calcium carbonate/sulfonate[20]) micelles. For zwitterionic micelles, a short description of a simulation of lysophosphatidylethanolamine[21] and a recent 1.2-ns simulation of a dodecylphosphocholine micelle are available.[22]

Here, we describe simulations of DPC micelles of three different sizes (40, 54, and 65 lipids), with a three-fold aim: (i) study the effect of aggregation size on the micelle structure, (ii) to compare the relaxation behavior of the lipid chains with NMR relaxation data, and (iii) to obtain a starting model and reference simulation for future work on DPC−peptide systems for a direct comparison with NMR experiments on peptides bound to DPC micelles. Recently, Wymore et al. simulated a DPC micelle consisting of 60 DPC lipids in water for 1.2 ns, providing another size in addition to the three in this paper.[22]

2. Methods

A single DPC molecule in the all-trans configuration was generated with a molecular editor (Figure 1). We built three micelles, of 40 (M40), 54 (M54), and 65 (M65) lipids, as follows: The input lipid molecule is rotated to lie along the *x* axis, with its last tail atom (C12) on the origin and C1 on the *x* axis. This molecule is copied and rotated n_ϕ times by $360/n_\phi$ degrees in the *xy* plane. The procedure is repeated with $2n_\theta$ planes parallel to the *xy* plane, but with the θ coordinates at $\pm 90/n_\theta$ degrees. The number of lipids in each plane is proportional to sin θ. For M65, this resulted in a micelle with 1, 3, 9, 13, 14, 13, 9, and 3 lipids in successive planes; for M54, 1, 7, 12, 14, 12, 7, and 1; and for M40, 4, 10, 12, 10, and 4. Finally, all lipids were translated by 0.5 nm in the radial direction to avoid overlap of van der Waals radii in the center of the micelle.

All simulations used the united-atom lipid parameters from ref 23 (set E). The charges on the phosphate group in DPC are

* Author to whom correspondence should be addressed. Current address: Laboratory of Molecular Biophysics, Rex Richards Building, University of Oxford, South Parks Road, Oxford OX1 3QU, U.K. Fax: +44-1865-275182. E-mail: tieleman@bioch.ox.ac.uk.

† University of Groningen.

‡ Biomedical Center.

10.1021/jp001268f CCC: $19.00
Published on Web 06/17/2000

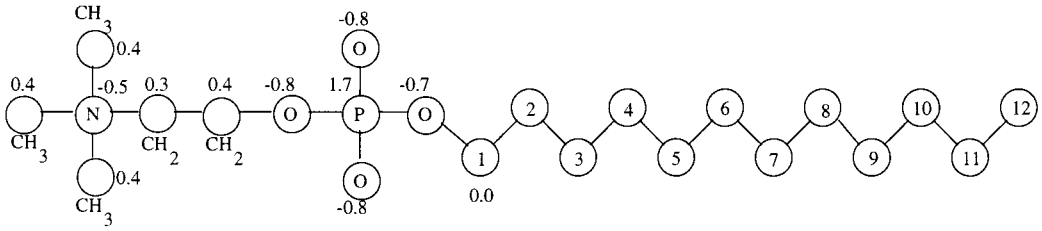

Figure 1. Structure of a dodecylphosphocholine molecule, with the charges and atom numbering used in this paper.

almost the same as ab initio derived charges for a monophosphate ion[24] (Figure 1).

The micelles were solvated with SPC water,[25] avoiding van der Waals overlap with lipid atoms and with increased radii of the tail atoms to avoid water molecules being placed in the core of the micelles. All three systems have a lipid:water ratio of 1:97. The systems were energy minimized and simulated for 50 ps with the lipid atoms harmonically restrained to their initial positions with a force constant of 200 kJ mol^{-1} to allow the water molecules to relax around the lipids. Temperature and pressure were controlled using the weak coupling method, at 300 K ($\tau_T = 0.1$ ps, lipids and solvent separately) and 1 bar ($\tau_p = 1.0$ ps), respectively.[26] A group-based twin-range cutoff for nonbonded interactions of 1.0/1.5 nm was used with a time step of 2 fs and with a neighborlist update every 10th step. Water bond lengths and angles were constrained using SHAKE,[27] and for the lipid bonds, a harmonic potential was used. After the restrained runs, we simulated the three systems without restraints for another 1050 ps. Analyses are based on the last 500 ps of the M40, M54, and M65 simulations. These simulations were run with the GROMACS software package[28] on our special-purpose parallel computer.[29] For the M54 micelle, an additional simulation of 14.4 ns, starting from the final structure after 1100 ps, was run using GROMACS on a single R10000 processor of an SGI Powerchallenge system. SETTLE[30] was used to constrain the water geometry, and LINCS to constrain the bond lengths in the lipids.[31] The time step was 5 fs with a neighborlist update every 4 steps. Such a large time step is possible using a special treatment of hydrogen atoms and yields stable trajectories for a small water-soluble protein even at time steps of 7 fs.[32] The other simulation parameters were the same as in the three previous runs. The inconsistent use of harmonic bonds, SHAKE, SETTLE, and LINCS is due to practical considerations but should not influence the results.[31] Our current algorithms of choice are SETTLE for SPC water and LINCS for bonds in all other molecules.

For comparison, we use earlier simulations of a DPPC bilayer and a decane liquid. The DPPC simulation has been described before in ref 23, set E. Briefly, the simulation contains 128 DPPC lipids and 3910 water molecules, has a length of 500 ps, a constant anisotropic pressure of 1.0 bar ($\tau_p = 1.0$ ps), a temperature of 325 K ($\tau_T = 0.1$ ps), time step of 2 fs, a neighborlist update every 10 steps, and a twin-range cutoff 1.0/2.0 nm for electrostatic interactions. The decane simulation consisted of 512 decane molecules at a constant isotropic pressure ($\tau_p = 1.0$ ps) and a temperature of 300 K ($\tau_T = 0.1$ ps), with a 1.0-nm cutoff, a 2-fs time step, and a neighborlist update every 10 steps. The density of decane was 0.745 (0.003) g cm^{-3}, using the same carbon parameters as for the lipid chains. The experimental density of decane at 293 K is 0.73 g cm^{-3}.

3. Results

3.1. Equilibration and Micelle Shape. The equilibration of the systems was monitored through the potential energy and the radius of gyration, as well as by visual inspection (Figure 2). After 600 ps, the radius of gyration, the potential energy, and its constituent terms were more or less stable. Further analyses were done on the last 500 ps of the trajectories. The 14.4-ns M54 trajectory was used to check convergence of structural properties for the M54 micelle and to analyze relaxation behavior (see below).

TABLE 1: Principal Moments of Inertia[a] Averaged over the Last 500 Picoseconds of the Simulations

	I_1	I_2	I_3	α^b
M65	4.77 ± 0.13	4.40 ± 0.08	4.01 ± 0.07	0.09 ± 0.02
M54	3.48 ± 0.06	3.35 ± 0.05	3.09 ± 0.08	0.05 ± 0.02
M40	2.32 ± 0.05	2.22 ± 0.06	1.70 ± 0.05	0.12 ± 0.02

[a] Moments of inertia in units of 10^4 amu nm^2. Asymmetry parameter, α, defined as $\alpha = (2I_1 - I_2 - I_3)/(I_1 + I_2 + I_3)$.

A logical property to consider when comparing the three different micelles is the potential energy and its constituent terms. After approximately 600 ps, the total potential energy becomes stable in all three simulations. However, the individual terms fluctuate significantly, even in the 14.4-ns run. The three simulations are directly comparable when all of the constituent potential energy terms are divided by 65, 54, and 40 for M65, M54, and M40, respectively. This results in energies per mole (DPC + 97 waters). The total potential energy difference between M54 and M40 averaged over 500 ps is less than 0.1%, which is not significant when considering the fluctuations present in the 14.4-ns simulation, although it appears significant when only the M40, M54, and M65 simulations are considered. Thus, the potential energy terms do not provide any clues about which micellar size might be most favorable.

A more detailed analysis of the shapes of the three micelles is possible for the principal moments of inertia (Table 1). These are averages over the diagonalized inertia tensor at each time step. The principal moments of inertia of M54 are the closest to each other, indicating a mostly spherical shape, with the principal moments of inertia in the ratio of 1.1:1.1:1. The values for M65 are somewhat further apart, with a ratio of 1.2:1.1:1. M40, however, has two similar values and one much lower component, indicating a shape like a prolate ellipsoid (ratio of 1.4:1.3:1). Figure 2 shows that, in M40 the lipids align into a small bilayer-like shape, with the headgroups collected on either side and a relatively large exposed hydrophobic surface in the middle.

Wymore et al. found a ratio of 1.2:1.1:1 for their DPC micelle with 60 lipids,[22] the same as the values for M65. However, these values are based on relatively short simulations (ca. 1 ns), because shape changes of the micelle as a whole are likely to occur mostly on time scales much longer than 1 ns. In Figure 3, the ratios I_1/I_3 and I_1/I_2 are plotted for the 14.4 ns of the M54 run. Even though the values appear to be stable for many nanoseconds, after about 8 ns, the micelle shape changes slowly to a less symmetrical structure. However, this does not seem to affect the local structure of the lipids significantly.

3.2. Interfacial Properties. The solvent accessible surface area per lipid is expected to depend on the aggregate size. In

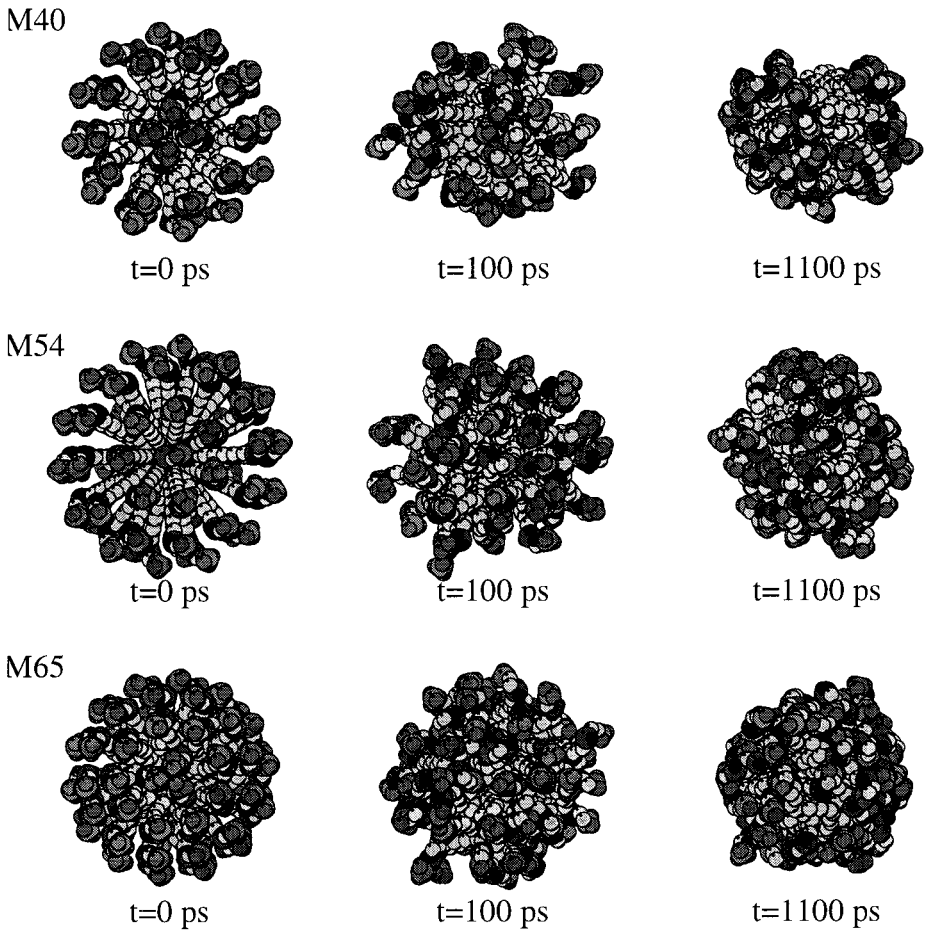

Figure 2. Snapshots at different times during the simulation.

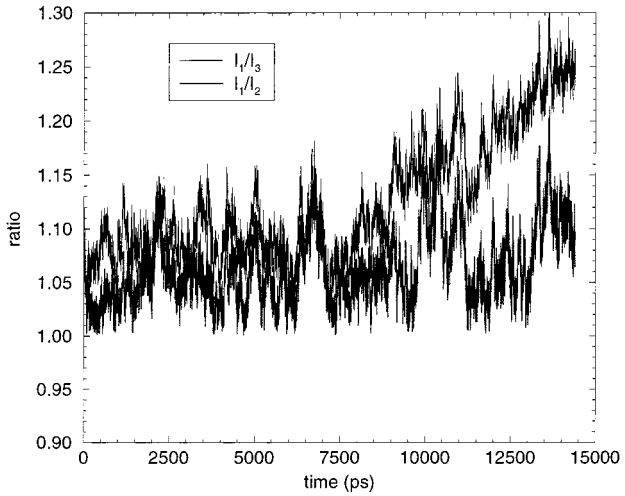

Figure 3. Ratios between the principal moments of inertia, calculated and sorted at every step.

Table 2, the solvent accessible surface area, calculated using GRASP[33] with a probe radius of 1.4 Å, is given for the whole lipids, the carbon tails, and the two halves of the tails. The area per molecule decreases from M40 to M54 to M65. The difference between M40 and the other two is especially large for the lipid tails. For comparison, the solvent accessible area per DPPC molecule in ref 23 (set E) was 1.85 nm^2. The solvent accessible area of the two palmitoyl tails was very small, less than 0.1 nm^2. This agrees with the observation that much less water penetrates past the carbonyl groups in DPPC than past the first carbon in the micelles.

TABLE 2: Solvent Accessible Surfaces Per Lipid for the Total Lipid, the C_{12} Chain, the First Eight Carbons, and the Last Four Carbons

system	total (nm^2)	tail (nm^2)	C1−C8 (nm^2)	C9−C12 (nm^2)
M65	1.68	0.33	0.23	0.10
M54	1.80	0.39	0.26	0.13
M40	2.01	0.52	0.32	0.20

The radial density of the system, solvent, lipids, and individual lipid atoms of M54 is given in Figure 4, where r is the distance from the center of mass of the micelle and a bin width of 0.1 nm was used. The interface between lipids and solvent is broad. The density for water at a given distance from the center of mass of the micelle drops from 90% to 10% (analogous to the definition of the width of the lipid−solvent interface in bilayers) over a distance of 0.9 nm. In DPPC bilayers, the interfacial width is about 1.2−1.3 nm. The tail atoms have a broad distribution, with significant overlap with the water distribution.

The DPC density begins to drop roughly at the maximum density of the P atoms in all three systems (which coincides with the maximum density of all atoms), at 1.76 ± 0.04, 1.68 ± 0.04, and 1.54 ± 0.04 nm for M65, M54, and M40, respectively. If each of these maxima is taken as the radius of a sphere (which is a somewhat arbitrary choice), an average area per lipid can be calculated. For M65, this gives an area of 0.60 ± 0.03 nm^2; for M54, 0.66 ± 0.03 nm^2; and for M40, 0.75 ± 0.04 nm^2. For DPPC the best available value is ca. 0.63 nm^2.[34]

One important phospholipid bilayer property for the binding of peptides and small molecules is a surface potential of several hundred millivolts, caused by the membrane lipids and water.[35]

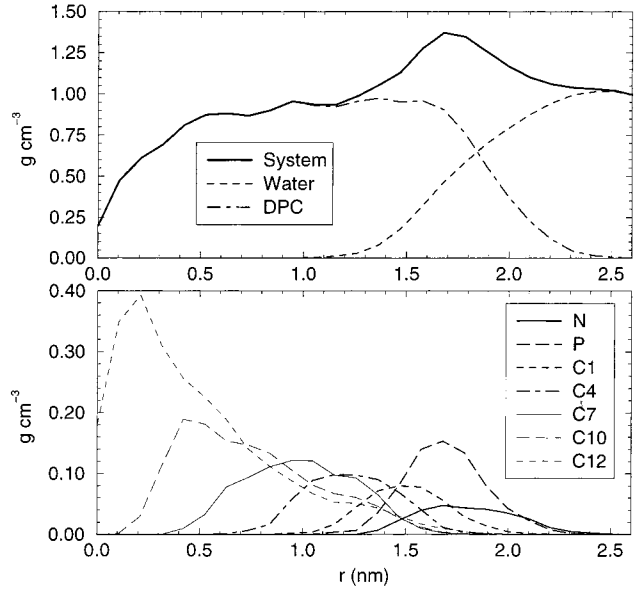

Figure 4. Radial density for the M54 system. In the top panel, the total density, the water density, and the lipid density are given; in the bottom panel, the densities of selected atoms are given.

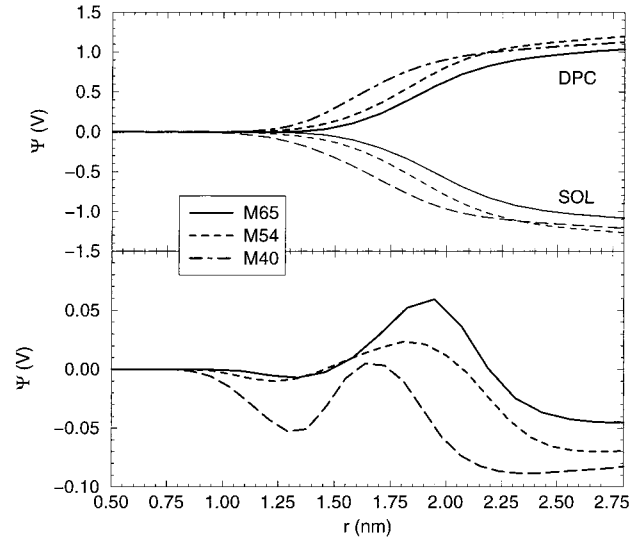

Figure 5. Electrostatic field and potential as a function of the distance from the center of the micelle. Top: Contribution to the electrostatic potential, as a function of the distance from the center of mass of the micelle, due to the lipid (DPC) and to water (SOL), for all three systems. Bottom: Total electrostatic potential for all three systems as a function of distance from the center of mass.

If a spherical symmetry is assumed, the electrostatic potential ψ is given by

$$\frac{1}{r}\frac{d^2(r\psi)}{dr^2} = -\rho(r)/\epsilon_0 \qquad (1)$$

where $\rho(r)$ is the charge density as function of the distance r from the micelle center and ϵ_0 is the dielectric constant of a vacuum. The zero of potential is taken at $r = 0$, and the field is zero at the center of the micelle (Figure 5). As was found for planar dipolar interfaces,[36] the charge density due to water dipoles overcompensates the charge density from the lipid headgroups, and the potential drops by ca. 50−100 mV across the lipid−water interface, the aqueous side being negative. This value may be an overestimation due to the neglect of electronic polarization.

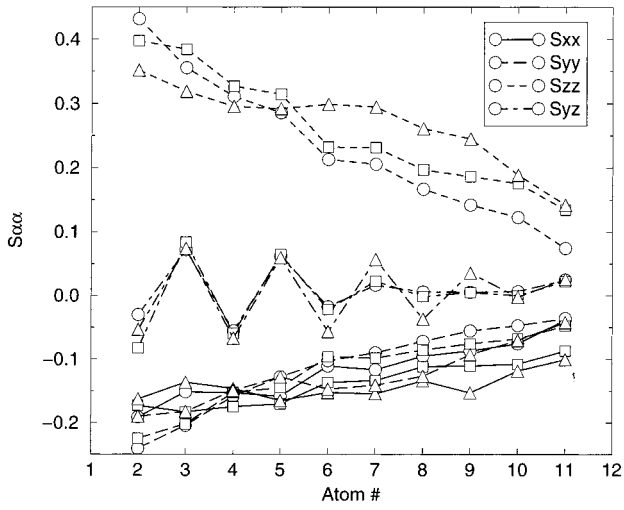

Figure 6. The order parameter tensor elements for the three micelles M40 (circles), M54 (squares), and M65 (triangles).

3.3 The Micelle Interior. An order parameter tensor can be defined via the orientation of the C−H bonds with respect to a director. In bilayers, the natural choice for the director is the axis perpendicular to the bilayer, but in the case of a micelle, the choice is somewhat arbitrary. We used the vector from the center of mass of the micelle to the phosphorus atom as the director. Then, the order parameter tensor S is given by

$$S_{ij} = \frac{1}{2}\langle 3\cos\theta_i \cos\theta_j - \delta_{ij}\rangle \qquad (2)$$

in which θ_i is the angle between the ith molecular axis and the director. The molecular axes for the nth CH_2 unit are

z: vector from C_{n-1} to C_{n+1}

y: vector $\perp$ to z and in the plane through C_{n-1}, C_n, and C_{n+1}, pointing from C_n away from $^1/_2(C_{n+1} + C_{n-1})$

x: vector $\perp$ to z and y

From the diagonal elements S_{xx}, S_{yy}, and S_{zz}, the deuterium order parameter S_{CD} can be calculated using

$$-S_{CD} = \frac{2}{3}S_{xx} + \frac{1}{3}S_{yy} \qquad (3)$$

but in micelles, there is no director related to the external magnetic field, and hence, no deuterium splitting is observed. Thus, a direct measurement of S_{CD} is impossible. However, S_{CD} follows from relaxation theory as a fitting parameter in measurements at different field strengths (see below and refs 10 and 37). If the motion of the lipids around the director is isotropic, then $S_{xx} = S_{yy}$, $S_{yz} = 0$, and $S_{zz} = -2S_{CD}$, the deuterium order parameter.[38] If the motion is not isotropic, then $S_{yz} \neq 0$, and its value alternates for successive bonds: the covalent bond between C_n and C_{n+1} enforces a relation between successive order parameters. In the simplified case that successive diagonal elements are equal, $S_{yz}^{(n+1)} = -S_{yz}^{(n)}$.

The four elements S_{xx}, S_{yy}, S_{zz}, and S_{yz} of this tensor are plotted for the three micelles in Figure 6. The diagonal elements S_{xy} and S_{xz} are zero because of symmetry. The order parameter profile values found are similar to values calculated from NMR relaxation measurements at different fields, using a simple two-step model to fit the data.[39] The values are also comparable to

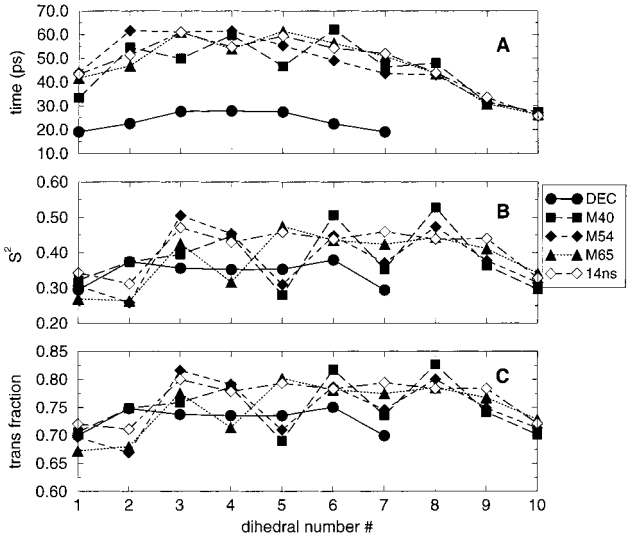

Figure 7. Dihedral properties of decane at 300K; the M40, M54, and M65 micelles, calculated over the last 600 ps of the trajectories; and the M54 14.4-ns simulation. The statistical error in the decane properties is less than 0.5%, of the 14.4-ns M54 micelle, less than 5%, and of the short runs, ca. 20%. Note that the first dihedral is O−C1−C2−C3, the last, C9−C10−C11−C12. (A) Mean times between dihedral transitions. (B) Dihedral order parameters (see text). (C) Dihedral trans fractions.

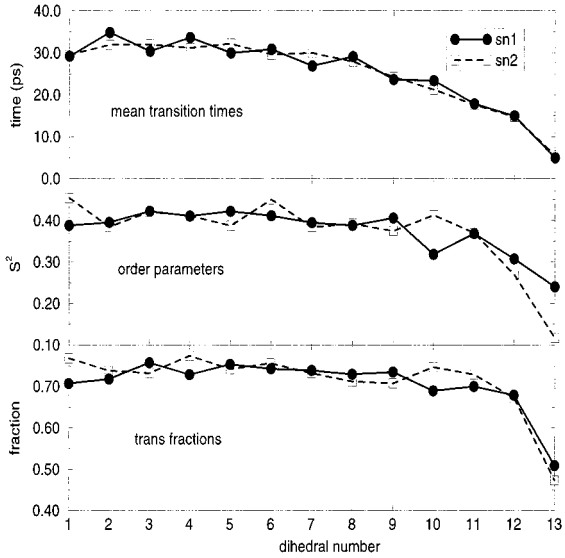

Figure 8. Dihedral transition times, dihedral order parameters, and trans fractions for DPPC at 325 K.

S_{CD} values found in the tails of DPPC bilayers.[36] The alternating S_{yz} values, being positive for odd-numbered C atoms, are compatible with a tilt of the chains with respect to the director, with the O−C bond being preferentially oriented along the director. Indeed, the average angle between the vector from the P atom to the last carbon of the lipid tail and our director between the P atom and the center of mass of the micelle is 36° ± 0.5° for M65, 38.3° ± 0.1° for M54, and 40° ± 0.5° for M40.

We analyzed the trans/gauche ratio, the average dihedral transition times of the tail dihedrals, and the dihedral order parameter S_D^2 as defined by Van der Spoel and Berendsen[40]

$$S_D^2 = C_D(\infty) = [\int_0^{2\pi} \cos(\theta)\, p(\theta)\, d\theta]^2 + [\int_0^{2\pi} \sin(\theta)\, p(\theta)\, d\theta]^2 \quad (4)$$

with $p(\theta)$ the dihedral distribution. S_D^2 is the value at infinite time of the correlation function

$$C_D(t) = \langle \cos[\theta(\tau) - \theta(\tau + t)] \rangle_\tau \quad (5)$$

The dihedral order parameter S_D^2 is a measure for the equilibrium distribution of the dihedral angle.[40] For the transition and trans-fraction calculations trans, gauche−, and gauche+ were each taken as a well with a width of 60°. A transition is counted if a dihedral changes from one potential well to another. This ensures that only real transitions are counted.

Figures 7 and 8 provide a summary of these three analyses for decane, M40, M54, M65, the 14.4-ns run, and DPPC.

In the four micelle systems, the transition time is comparatively short for the first dihedral angle; it then has a plateau value of 50−60 ps and drops toward 25 ps at the end of the tail. This picture can be compared to that calculated for a DPPC bilayer (Figure 8), in which the mean time between dihedral transitions is approximately 30 ps for the first eight dihedrals and then gradually drops toward the middle of the bilayer. In decane, the mean time between transitions is between 15 ps at the ends of the chain and 20 ps in the middle at 325 K (the temperature of the DPPC simulation, not shown) and between 20 ps at the ends and 30 ps in the middle at 300 K. The slower dihedral transitions in the DPC micelles compared to those in neat alkanes were also found by MacKerell for an SDS micelle[16] but not by Wymore et al. for a DPC micelle.[22] They attributed this to a lack of sampling in MacKerell's simulation (which was 120 ps), but lack of sampling is not an issue for transition times on the order of 100 ps in the long simulation in this paper. Venable et al. found similar transition rates for DPPC and hexadecane,[41] comparable to the agreement in transition rates between decane and the last 10 carbons of DPPC chains here. The mean dihedral transition time decreases toward the end of the chain (the core of the micelle), but not as drastically as in the simulation of Wymore et al. Overall, the chain properties are closer to those of a liquid crystalline lipid bilayer than to those of a lipid bilayer in the gel phase.

For the M40 system, there is a strong alternation in transition rates for the even and odd dihedral angles. To a lesser extent, such an alternation is also found in the other systems, notably also in the sn1 chain of DPPC. This has also been observed in a simulation of *n*-decyltrimethylammonium chloride micelles.[19] It is caused by a preferential tilt of the lipid chains with respect to the normal on the micelle surface, due to geometrical constraints.

A more static picture is provided by the average trans fractions and the dihedral order parameters along the lipid chains. The fluctuations along the chain are larger than for the mean dihedral transition times, but the difference between the different systems is smaller. The M65 system shows a strong alternation over the first five dihedral angles in both the dihedral order parameters and the trans fractions, whereas the M40 system has a strong alternation over dihedral angles 4− 9. The M54 system shows a smoother curve with a slight dip in the middle, which is no longer present in the 14.4-ns simulation. It appears that the equilibrium conformation of the lipid chains is comparable in the three different environments, micelle, bilayer, and decane, although the dynamics are different in the micelle.

3.4. Relaxation. In NMR relaxation experiments, the relaxation of a relevant bond is determined by the bond's orientational fluctuations with respect to the external magnetic field. To obtain the complete correlation function, one would need to perform measurements at a large number of magnetic field strengths,

but from a simulation, this function can be calculated directly from a sufficiently long trajectory. The total correlation function is given by[37]

$$C(t) = \frac{1}{5}\langle P_2[\hat{\mu}_{LF}(0)\cdot\hat{\mu}_{LF}(t)]\rangle \quad (6)$$

where the unit vector $\hat{\mu}_{LF}$ is the vector connecting the two nuclei in the laboratory frame of reference. P_2 is the second Legendre polynomial

$$P_2(x) = \frac{1}{2}(3x^2 - 1) \quad (7)$$

The spectral density, which determines the experimental observables T_1, T_2, and NOEs, is given by the Fourier cosine transform of $C(t)$.

$$J(\omega) = 2\int_0^\infty \cos(\omega t)\, C(t)\, dt \quad (8)$$

For $^{13}C-H$ dipolar relaxation, $\hat{\mu}$ is simply the CH vector. In this case, the spin−lattice relaxation time T_1 is given by

$$\frac{1}{NT_1} = \frac{1}{4}\left[\left(\frac{\mu_0}{4\pi}\right)\frac{\hbar\gamma_C\gamma_H}{r_{CH}^3}\right]^2 [J(\omega_H - \omega_C) + 3J(\omega_C) + 6J(\omega_C + \omega_H)] \quad (9)$$

and T_2 is given by

$$\frac{1}{NT_2} = \frac{1}{8}\left[\left(\frac{\mu_0}{4\pi}\right)\frac{\hbar\gamma_C\gamma_H}{r_{CH}^3}\right]^2 [4J(0) + J(\omega_H - \omega_C) + 3J(\omega_C) + 6J(\omega_H) + 6J(\omega_C + \omega_H)] \quad (10)$$

Here, N is the number of hydrogens bonded to the carbon, γ_C, γ_H, ω_C, and ω_H are the gyromagnetic ratios and Larmor frequencies for the ^{13}C and ^1H nuclei, respectively, and r_{CH} is the CH distance, which we assume to be fixed at 0.108 nm. We assume that, for ^{13}C relaxation, chemical shift anisotropy effects are negligible, even for measurements on 500-MHz NMR machines.

For the interpretation of relaxation data, in many cases, the assumption can be made that the total correlation function $C(t)$ can be split into two independent parts, one describing internal and one describing overall motion

$$C(t) = C_O(t)C_I(t) \quad (11)$$

with

$$C_O(t) = \frac{1}{5}e^{-6D_M t} = \frac{1}{5}e^{-t/\tau_M} \quad (12)$$

and the internal part

$$C_I(t) = \langle P_2[\hat{\mu}(0)\cdot\hat{\mu}(t)]\rangle \quad (13)$$

Now, $\hat{\mu}$ describes the orientation of the interaction vector in a frame of reference rigidly attached to the macromolecule.

Lipari and Szabo[37] and Wennerström et al.[10] have suggested a simple two-step model to interpret NMR relaxation data. In this formalism, $C_I(t)$ is approximated by

$$C_I(t) = S^2 + (1 - S^2)e^{-t/\tau_e} \quad (14)$$

Here, S^2 is a generalized order parameter and τ_e is an effective correlation time for all motions that are fast compared to the Larmor frequency. S^2 is defined as $C_I(\infty)$, and τ_e is defined via the equation

$$\tau_e(1 - S^2) = \int_0^\infty [C_I(t) - S^2]\, dt \quad (15)$$

For bilayers, S is the same as S_{CD}, the deuterium order parameter determined from observed deuterium splittings.

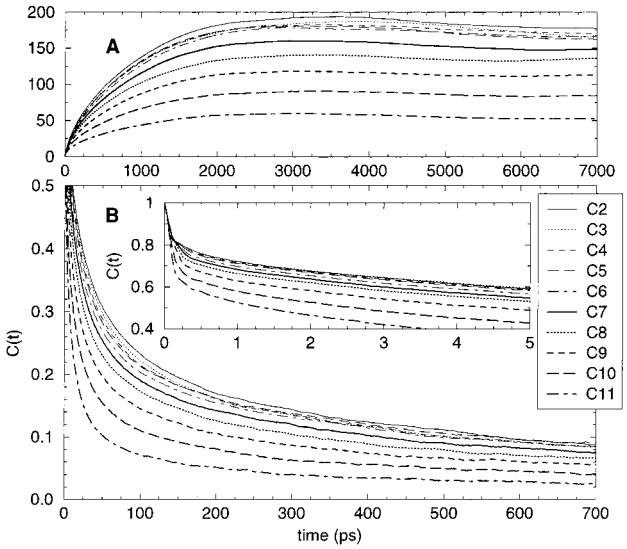

Figure 9. (A) Integral over the correlation function $C(t)$ for carbons 2−11. (B) Correlation function $C(t)$ at two different time spans for carbons 2−11.

In a micelle, no rigidly attached frame of reference can be defined, and consequently, the internal and external correlation functions cannot be rigorously separated. Internal motions mix with lipid diffusion, lipid rotation, and rotational diffusion of the micelle as a whole. However, in principle, the overall correlation function $C(t)$ can be calculated from a simulation, provided that the length of the simulation is sufficient. Because we used a united-atom model for the carbon chains, we have to "generate" hydrogens, constructing idealized CH vectors from the positions of the carbon atoms. We assume that deviations from the normal tetrahedral geometry due to bond and angle variations are small and can be neglected. In Figure 9, the overall orientational correlation function

$$C(t) = \langle P_2[\hat{\mu}_{LF}(0)\cdot\hat{\mu}_{LF}(t)]\rangle \quad (16)$$

is plotted for carbons 2−11 along the chain, averaged over all 54 lipids. It was calculated with a fast Fourier transform method on 14 400 points in the trajectory.

In principle, $C(t)$ for a micelle, which has no residual anisotropy like a bilayer, can be fit by an infinite sum of exponential functions.

$$C(t) = \sum_{i=0}^{\infty} a_i \exp\left(\frac{-t}{\tau_i}\right) \quad (17)$$

The program DISCRETE[42] (version 2, 1990) was used to fit a sum of exponentials to the calculated correlation functions. DISCRETE uses a transform that maximizes the Fisher information content and automatically estimates the number of exponentials that best fit the data. For fitting, the data were sampled as follows: the first 16 points were all used; of the next 32, every second point was used; of the next 64, every fourth point, of the next 128, every eighth; and so on, resulting in 156 points in total. The baseline component a_0 was set to 0.

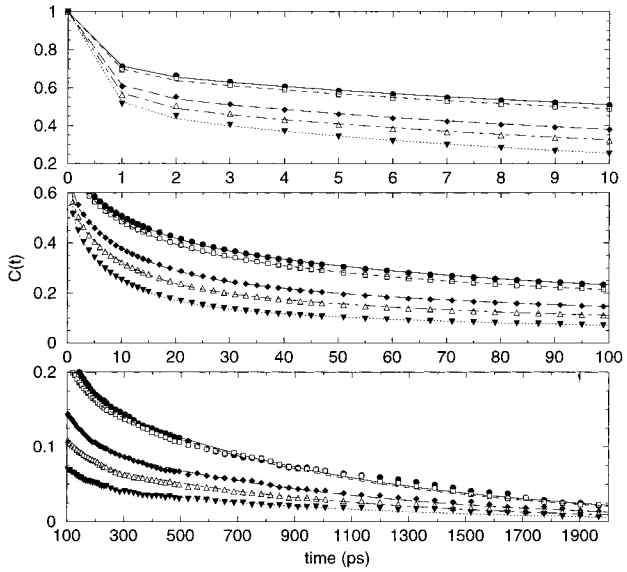

Figure 10. Four-exponential fit to the autocorrelation functions for carbons 2 (black circle, solid line), 5 (white square, dashed line), 9 (black diamond, long dashed line), 10 (white triangle, dot-dashed line), and 11 (black triangle, dotted line) at three different time scales. Symbols are points from the calculated correlation functions, lines are the fitted functions. See Table 3 for all fitted values.

TABLE 3: Parameters of a Fit of Four Exponentials to the Rotational Autocorrelation Function

carbon	τ_1 (ps)	τ_2 (ps)	τ_3 (ps)	τ_4 (ps)	a_1	a_2	a_3	a_4
2	0.487	10.395	67.889	926.784	0.299	0.248	0.260	0.193
3	0.495	11.270	70.323	952.381	0.301	0.261	0.260	0.178
4	0.481	10.934	65.466	945.448	0.308	0.263	0.249	0.181
5	0.481	9.978	56.051	900.820	0.313	0.247	0.248	0.192
6	0.481	10.268	59.923	951.384	0.329	0.261	0.232	0.178
7	0.481	10.353	63.335	925.754	0.347	0.271	0.220	0.162
8	0.484	10.589	71.276	914.913	0.376	0.287	0.196	0.140
9	0.481	9.764	64.098	906.125	0.407	0.288	0.186	0.119
10	0.481	8.756	56.054	874.279	0.451	0.286	0.171	0.091
11	0.481	8.114	53.969	889.759	0.496	0.320	0.126	0.057

TABLE 4: Parameters of a Fit of Three Exponentials to the Rotational Autocorrelation Function

carbon	τ_1 (ps)	τ_2 (ps)	τ_3 (ps)	a_1	a_2	a_3
2	1.028	34.141	765.111	0.378	0.387	0.227
3	1.002	31.289	759.301	0.374	0.403	0.215
4	0.943	31.289	772.201	0.379	0.400	0.214
5	0.892	29.240	773.395	0.385	0.393	0.217
6	0.880	28.531	792.393	0.401	0.388	0.206
7	0.857	27.655	738.007	0.419	0.381	0.195
8	0.808	25.374	663.130	0.445	0.369	0.182
9	0.754	22.978	643.915	0.477	0.364	0.156
10	0.695	19.782	580.046	0.520	0.352	0.125
11	0.602	14.057	462.321	0.550	0.358	0.091

The best fit was obtained by a fit to a sum of four exponentials (eight parameters). The fitted values are given in Table 3 and Figure 10. For all carbons, there is a very fast component (<0.5 ps), a component with $\tau \approx 10$ ps, a component with $\tau \approx 50-70$ ps, and a slow component with $\tau \approx 900$ ps. The last carbons of the lipid chains have significantly shorter time constants for the three slowest components compared to those of carbons closer to the headgroup. A fit to a sum of three exponentials also gives a reasonable fit, but deviates at intermediate times from the original data (Table 4). A fit to more exponentials obviously can also describe the calculated correlation functions but just means a redistribution of the intermediate τ_i values over more parameters. We do not propose a model or molecular interpretation of the calculated exponential decay constants, but merely use them as a convenient analytical form of $C(t)$ for the calculation of spectral densities.

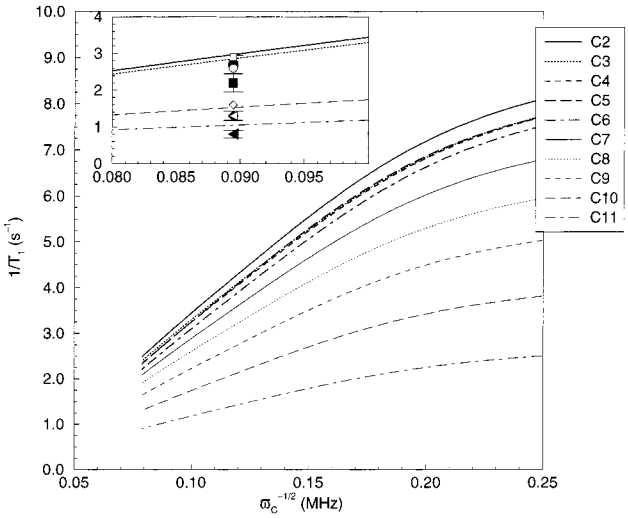

Figure 11. Calculated T_1 values as a function of $1/\sqrt{\omega_C}$. The inset shows experimental measurements for $\omega_C = 125$ MHz, at pH 5 and 12 °C (open symbols) and at pH 3 and 25 °C (filled symbols). Error bars on the open symbols have been omitted but are roughly of the same magnitude as those for the closed symbols. Circles, C2; squares, C3; diamonds, C10; and triangles, C11.

TABLE 5: Calculated and Experimental T_1 and T_2 Values for ^{13}C Relaxation at $\omega_C = 125$ MHz[a]

	$1/T_1$ (s^{-1})			$1/T_2$ (s^{-1})		
carbon	pH 5, 12 °C	pH 3, 25 °C	sim	pH 5, 12 °C	pH 3, 25 °C	sim
α	2.8	2.2	4.3	9.5	7.5	14.0
2	2.8	2.7	2.9	10.0	8.0	9.5
3	2.9	2.2	2.7	7.8	7.0	9.0
10	1.6	1.3	1.5	7.9	5.8	4.7
11	1.3	0.8	1.0	5.4	4.7	3.2

[a] Experimental data from ref 44. The statistical error in the simulation is ca. 5−10% (based on the quality of the experimental fits). The experimental error is about 10%.

The four-exponential fit can be used to calculate the T_1 and T_2 relaxation times as a function of the external field using eqs 9 and 10. The Fourier cosine transform of the fitted function is just a sum of four Lorentzians and can be readily calculated. The predicted frequency dependence of T_1 is plotted in Figure 11. Beswick et al. measured T_1 and T_2 ^{13}C relaxation times at pH 5, 12 °C, and at pH 3, 25 °C at a carbon frequency $\omega_C = 125$ MHz. These values are given in Figure 11 (T_1) and Table 5. The agreement between the calculated and experimental T_1 and T_2 values is reasonable for the chains, but less so for the headgroup Cα, the carbon neighboring the phosphate group. T_2 contains $J(0)$, the integral over the correlation function $C(t)$, and can therefore be calculated less accurately than T_1, which mainly depends on faster local motions.

The original $C(t)$ function itself goes to zero rapidly, as can be seen from the integral of these functions in Figure 9. At ca. 5 ns, the integrals reach a plateau, although they continue to rise in particular after 7 ns, at which point the correlation functions become too noisy to be reliable. This noise prevents a direct Fourier transform of $C(t)$ in place of the fitted exponentials. Surprisingly, $C(t)$ decays too rapidly to contain major contributions from slower motions such as lipid diffusion and rotation of the micelle as a whole. Although these motions are on the same time scale as the simulation length of 14.4 ns, we can try to estimate them.

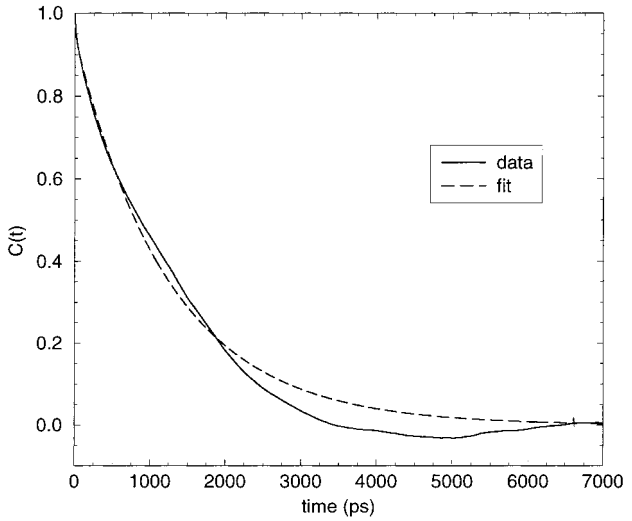

Figure 12. Autocorrelation function of the vector from the P atom to C10 in the tail, plus a fit of two exponentials to this function.

The motion of a single lipid as a whole can be characterized by the correlation function of a vector that is, on average, the molecular axis of a lipid, which we took as the vector between the P atom and C10. Taking C12 or C8 does not significantly change the results. The orientational correlation function for this vector is given in Figure 12. Fitting this function with DISCRETE yields two possible solutions. One is a two-exponential fit with a very small fast component ($a_1 = 0.05$, $\tau_1 = 16$ ps) and a large component with $\tau \approx 1.3$ ns. The second is a single-exponential fit with $\tau \approx 1.2$ ns. This motion will contribute to the slowest component of the overall relaxation function $C(t)$. However, the fit is not very good, because the correlation function itself is negative for hundreds of picoseconds, and the integral over the fitted function is larger than the integral over the real correlation function.

The overall motion of a rigid spherical body in a fluid with viscosity η is given by

$$\tau_R = \frac{4\pi a^3 \eta}{3kT} \tag{18}$$

Using the calculated viscosity[43] of SPC at 300 K of $\eta = 5.5 \times 10^{-4}$ kg m^{-1} s^{-1} and assuming a radius of 2.0 nm (based on the density profile in Figure 4 plus some bound water molecules), $\tau_R \approx 4.5$ ns. This value is rather approximate because the micelle is not a spherical rigid body, it is hard to estimate the effective hydrodynamic radius of the lose aggregate with bound water, overall rotation cannot be rigorously separated from lipid diffusion, and rotation of the lipid aggregate is hindered by the periodic boundary conditions, effectively increasing the viscosity of water. The value of $\tau_R = 4.5$ ns can be considered a lower bound. Using an experimentally estimated hydrodynamic radius of 2.3 or 2.7 nm (different methods[5]) and the experimental viscosity of water, the overall correlation time would be much larger.

4. Discussion

4.1. Micelle Size and Shape. Experimentally various physicochemical properties of DPC micelles have been determined using quasi-elastic light scattering (LS), analytical ultracentrifuge (UC),[5] and NMR Fourier transform pulsed-field-gradient spin echo (PGSE).[6] LS and PGSE measure the diffusion coefficient of the micelles. From the diffusion coefficients, diameters of spheres of an equivalent hydrodynamic radius are usually derived. Because the diffusion coefficients are for the micelle/bound water complex, the radius obtained from them will include bound water. This causes a significant inaccuracy in the determination of the micelle aggregation number. PGSE gave a micelle size of 44 ± 5, UC and LS, 56 ± 5. Because it is assumed that the distribution of micelle sizes is fairly sharply peaked, we chose three different micelle sizes around these experimentally determined sizes.

The actual shapes of the micelles in the simulation and the solvent accessible hydrophobic area suggest that M40 is too small, although it can be a short-lived intermediate structure. The differences in calculated properties for M54 and M65 are small. Potential energies in each system are too similar to estimate which aggregate size is most favorable. In the end, the energetic balance between the various contributions to the potential energy and the entropic effects of the lipid configurations plus the water around the micelles is very subtle. M40, in particular, provides an interesting view of the conflicting tendencies of headgroup−headgroup interactions, chain packing, and water-chain interactions.

4.2. The Micelle/Water Interface. Similar to the lipid/water interface in bilayers, the interface between lipids and solvent in the micelles is rough. In this respect, the zwitterionic DPC micelles are not different from the other types of micelles in previous simulations[16−20] or the DPC micelle of Wymore et al.[22] Although the atom distribution was only shown for M54, the other two give similar results. The distribution is broadest for the last carbons of the tails, which is logical, considering the spherical shape of the micelle and the fact that the headgroups must be near the surface. Water penetration to the core of the micelle is not observed. With the similarity between the DPC headgroups and phosphatidylcholine headgroups and the similar water orientation as judged from the electrostatic potential profile across the interface, the water/lipid interface of a DPC micelle resembles that of a DPPC lipid bilayer. However, a peptide, in particular an amphipathic peptide, is likely to significantly change the preferred number of lipids in a micelle.[44] Kallick et al.[6] and Fletcher and Keire[8] have already commented on concentration effects and differences in structures for a peptide on different types of micelles.[8] Simulations of peptides bound to a bilayer and to DPC micelles might be useful to elaborate on this. A first step in that direction has already been made by Wymore et al.[22,45] who studied a peptide bound to an SDS micelle.

4.3. Chain Properties. The dihedral trans and gauche fractions, dihedral order parameters, and CH_2 order parameters in the micelles are comparable to those found in lipid bilayers. The dihedral order parameters are a measure of the shape of the dihedral distribution, which turns out to be similar in different environments. However, a significant difference between the micelles and the DPPC bilayer is the much slower dihedral transition rate in the micelle. This was also found by MacKerell in a simulation of a sodium dodecyl sulfate micelle,[16] but not by Wymore et al. in a simulation of the same DPC micelle.

The long simulation of M54 turns out to be, somewhat surprisingly, sufficient to calculate the full correlation function of CH vectors in the lipid chains. These correlation functions can be fit with a sum of four exponentials, with the slowest component being on the order of 1 ns. From the fits or the original function, T_1 relaxation times can be calculated as a function of the ^{13}C frequency (or equivalently, the strength of the magnetic field). There is no need to take into account slow

motions involving the whole micelle for the calculation of the spectral densities.[39] Because the overall and internal motions of micelle rotation, lipid diffusion, lipid rotation, dihedral transitions, and faster motions are coupled in a micellar aggregate, it is not possible to separate the orientational CH correlation functions into an internal and an external part. The two-step model of Lipari and Szabo is not applicable in this case.[37] It would be of great interest to have detailed experimental data on DPC micelles at different field strengths.

5. Conclusion

We have described three DPC micelles of different sizes. Some properties suggest that the smallest one is least favorable, but it is difficult to discriminate between M54 and M65. In solution, all three will occur, although the distribution of micelle sizes is assumed to be fairly homogeneous, based on experimental measurements. An interesting extension of the current work would be to estimate the free energy difference between the different micelle sizes to determine the shape of the distribution. This might be done by creating or annihilating a lipid in micelles of different sizes, although this would be computationally very expensive and possibly not accurate enough to distinguish between micelles that differ by only a few lipids in size.

A simulation of 15 ns allows the complete calculation of the CH vector orientational correlation functions in this particular system. From these correlation functions, the spectral densities can be calculated and, through these, the T_1 and T_2 relaxation times. In particular, the calculated relaxation times for the lipid chains agree well with experimental values. Molecular dynamics simulations are approaching a time scale at which experimentally determined relaxation phenomena can be calculated directly, without the need for motional models.

Finally, the micelle simulations can be used as a reference for further work on peptide−lipid interactions, similar to simulations of peptides and proteins in lipid bilayers.[46] Efforts in that direction are currently being made, using structures from the M54 simulation.

Acknowledgment. We thank Drs. R. Scheek, S.J. Marrink, and R. Pastor for critical comments on an earlier version of the manuscript. D.P.T. was supported in part by the Research Council for Chemical Research (CW) with a subsidy from The Netherlands Organization for Scientific Research (NWO) and from Unilever Research, Vlaardingen, The Netherlands. D.P.T. thanks EMBO for a long-term fellowship. D.v.d.S. was supported by NWO.

References and Notes

(1) Rigaud, J. L.; Pitard, B.; Levy, D. *Biochim. Biophys. Acta*. **1995**, *1231*, 223−246.
(2) Jap, B. K.; Zulauf, M.; Scheybani, T.; Hefti, A.; Baumeister, W.; Aebi, U.; Engel, A. *Ultramicroscopy* **1992**, *46*, 45−84.
(3) Brown, L. R. *Biochim. Biophys. Acta*. **1979**, *557*, 135−48.
(4) Henry, G. D.; Sykes, B. D. *Methods Enzymol.* **1994**, *239*, 515−535.
(5) Lauterwein, J.; Bösch, C.; Brown, L. R.; Wüthrich, K. *Biochim. Biophys. Acta* **1979**, *556*, 244−264.
(6) Kallick, D. A.; Tessmer, M. R.; Watts, C. R.; Li, C-Y. *J. Magn. Reson. B* **1995**, *109*, 60−65.
(7) Dauplais, M.; Neumann, J. M.; Pinkasfeld, S.; Menez, A.; Roumestand, C. *Eur. J. Biochem.* **1995**, *230*, 213−220.
(8) Fletcher, T. G.; Keire, D. A. *Protein Sci.* **1997**, *6*, 666−675.
(9) van den Hooven, H. W; Spronk, C. A. E. M.; van de Kamp, M.; Konings, R. N. H.; Hilbers, C. W.; van de Ven, F. J. M. *Eur. J. Biochem.* **1996**, *235*, 394−403.
(10) Wennerström, H.; Lindman, B.; Söderman, O.; Drakenberg, T.; Rosenholm, J. B. *J. Am. Chem. Soc*. **1979**, *101*, 6860−6864.
(11) Chevalier, Y.; Cachaty, C. *J. Phys. Chem.* **1985**, *89*, 875−880.
(12) Söderman, O.; Walderhaug, H.; Henriksson, U.; Stilbs, P. *J. Phys. Chem.* **1985**, *89*, 3693−3701.
(13) Bendedouch, D.; Chen, S.-H.; Koehler, W. C. *J. Phys. Chem.* **1983**, *87*, 153−159.
(14) Holler, F.; Callis, J. B. *J. Phys. Chem.* **1989**, *93*, 2053−2058.
(15) Brown, M. F.; Seelig, J.; Häberlen, U. *J. Chem. Phys.* **1979**, *70*, 5045−5053.
(16) Mackerell, A. D., Jr. *J. Phys. Chem.* **1995**, *99*, 1846−1855.
(17) Jönsson, B.; Edholm, O.; Teleman, O. *J. Chem. Phys.* **1986**, *85* (4), 2259−2271.
(18) Shelley, J. C.; Sprik, M.; Klein, M. L. *Langmuir* **1993**, *9*, 916−926.
(19) Boecker, J.; Brickmann, J.; Bopp, P. *J. Phys. Chem.* **1994**, *98*, 712−717.
(20) Tobias, D. J.; Klein, M. L. *J. Phys. Chem.* **1996**, *100*, 6637−6648.
(21) Wendoloski, J. J.; Kimatian, S. J.; Schutt, C. E.; Salemme, F. R. *Science* **1989**, *243*, 636−638.
(22) Wymore, T.; Gao, X. F.; Wong, T. C. *J. Mol. Struct.* **1999**, *485*−*486*, 195−210.
(23) Tieleman, D. P.; Berendsen, H. J. C. *J. Chem. Phys.* **1996**, *105*, 4871−4880.
(24) van der Spoel, D.; Feenstra, K. A.; Hemminga, M. A.; Berendsen, H. J. C. *Biophys. J.* **1996**, *71*, 2920−2932.
(25) Berendsen, H. J. C.; Postma, J. P. M.; Gunsteren, W. F.; Hermans, J. Interaction Models for Water in Relation to Protein Hydration. In *Intermolecular Forces*; Pullman, B., Ed.; Reidel: Dordrecht, The Netherlands, 1981; pp 331−342.
(26) Berendsen, H. J. C.; Postma, J. P. M.; van Gunsteren, W. F.; DiNola, A.; Haak, J. R. *J. Chem. Phys.* **1984**, *81*, 3684−3689.
(27) Ryckaert, J. P.; Ciccotti, G.; Berendsen, H. J. C. *J. Comput. Phys.* **1977**, *23*, 327−331.
(28) van der Spoel, D.; van Buuren, A. R.; Apol, E.; Meulenhoff, P. J.; Tieleman, D. P.; Sijbers, A. L. T. M.; Hess, B.; Feenstra, K. A.; van Drunen, R.; Berendsen, H. J. C. *GROMACS 2.0 Manual*; University of Groningen: Groningen, The Netherlands, 1996. Internet: http://rugmd0.chem.rug.nl/∼gmx.
(29) Berendsen, H. J. C.; van der Spoel, D.; van Drunen, R. *Comput. Phys. Commun.* **1995**, *91*, 43−56.
(30) Miyamoto, S.; Kollman, P. A. *J. Comput. Chem.* **1992**, *13*, 952−962.
(31) Hess, B.; Bekker, H.; Berendsen, H. J. C.; Fraaije, J. G. E. M. *J. Comput. Chem.* **1997**, *18*, 1463−1472.
(32) Feenstra, K. A.; Hess, B.; Berendsen, H. J. C. *J. Comput. Chem.* **1999**, *20*, 786−798.
(33) Nicholls, A.; Sharp, K.; Honig, B. *Proteins: Struct., Funct., Genet.* **1991**, *11*, 281.
(34) Nagle, J. F.; Zhang, R.; Tristram-Nagle, S.; Sun, W. J.; Petrache, H. I.; Suter, R. M. *Biophys. J.* **1996**, *70*, 1419−1431.
(35) Cevc, G. *Biochim. Biophys. Acta* **1990**, *1031*, 311−382.
(36) Tieleman, D. P.; Marrink, S. J.; Berendsen, H. J. C. *Biochim. Biophys. Acta* **1997**, *1331*, 235−270.
(37) Lipari, G.; Szabo, A. *J. Am. Chem. Soc.* **1982**, *104*, 4546−4559.
(38) van der Ploeg, P.; Berendsen, H. J. C. *Mol. Phys.* **1982**, *49*, 243−248.
(39) Walderhaug, H.; Söderman, O. *J. Phys. Chem.* **1984**, *88*, 1655−1662.
(40) van der Spoel, D.; Berendsen, H. J. C. *Biophys. J.* **1997**, *72*, 2032−2041.
(41) Venable, R. M.; Zhang, Y.; Hardy, B. J.; Pastor, R. W. *Science* **1993**, *262*, 223−226.
(42) Provencher, S. W.; Vogel, R. H. *Math. Biosci.* **1980**, *50*, 251−262.
(43) Smith, P. E.; van Gunsteren, W. F. *Chem. Phys. Lett.* **1993**, *215* (4), 315−318.
(44) Beswick, V.; Guerois, R.; Cordier-Ochsenbein, F.; Coïc, Y.; Huynh-Dinh, T.; Tostain, J.; Noël, J.; Sanson, A.; Neumann, J. *Eur. Biophys. J.* **1998**, *28*, 48−58.
(45) Wymore, T.; Wong, T. C. *Biophys. J.* **1999**, *76*, 1213−1227.
(46) Forrest, L. R.; Sansom, M. S. P. *Curr. Opin. Struct. Biol.* **2000**, *10*, 174−181.